Available on CMS information server **CMS AN 2006/072**

CMS Analysis Note

The content of this note is intended for CMS internal use and distribution only

25 April 2006

Differential jet cross sections at high p_{T}

A. Oehler, K. Rabbertz

Institut für Experimentelle Kernphysik, Universität Karlsruhe, Germany

CMS Collaboration

Abstract

In this study differential cross sections of jets with high transverse momentum ranging from $80\ \mathrm{GeV}$ up to $4000\ \mathrm{GeV}$ are presented. Two jet algorithms have been chosen, a k_{T} and a midpoint cone type algorithm. The jets are reconstructed from calorimeter towers of fully simulated events. Subsequently, they are calibrated employing a simple Monte-Carlo calibration technique [1] as well as corrected for detector effects. The by far dominant experimental uncertainty is due to the jet energy scale that has been varied by $\pm 3\%$ in order to estimate the impact on the cross section determination. Starting at about 15% at low transverse momenta it increases up to about 50% at the highest p_{T} and shows a similar behaviour in comparison to Tevatron results [2, 3].

In a similar way, the two chosen jet algorithms are applied to calculations of perturbative QCD in leading and next-to-leading order. The theoretical uncertainty here is dominated by the uncertainty of the input parton distribution functions of the proton and has been deduced by an evaluation of the error sets of the CTEQ6M [4] parton densities. Rising in p_{T} it ranges from about 5% with a minimum of 3% at $\approx 200\ \mathrm{GeV}$ up to $+65\%$ and -30% at the highest transverse momenta and is of the same order of magnitude as the experimental uncertainty.

1 Introduction

With the start-up of LHC, a new frontier of energy will be surpassed and it is not at all clear that an extrapolation of our current knowledge in the form of the Standard Model will suffice to describe the new measurements. Beginning with the first day of data taking, even in a phase with a rather low luminosity, studies of jet physics in the framework of quantum chromodynamics (QCD) will allow to check our current theory against the new data. In figure 1 the expected statistical uncertainties[1)] on jet cross sections are presented for a pilot run with $0.1\ \mathrm{fb}^{-1}$ and for a first physics run with $10\ \mathrm{fb}^{-1}$ demonstrating that even up to $1.5\ \mathrm{TeV}$ sufficient statistics will be available. A profound understanding of QCD and jet physics is mandatory to establish phenomena beyond the standard model. In addition, jets are an indispensable tool to improve our understanding of the detector.

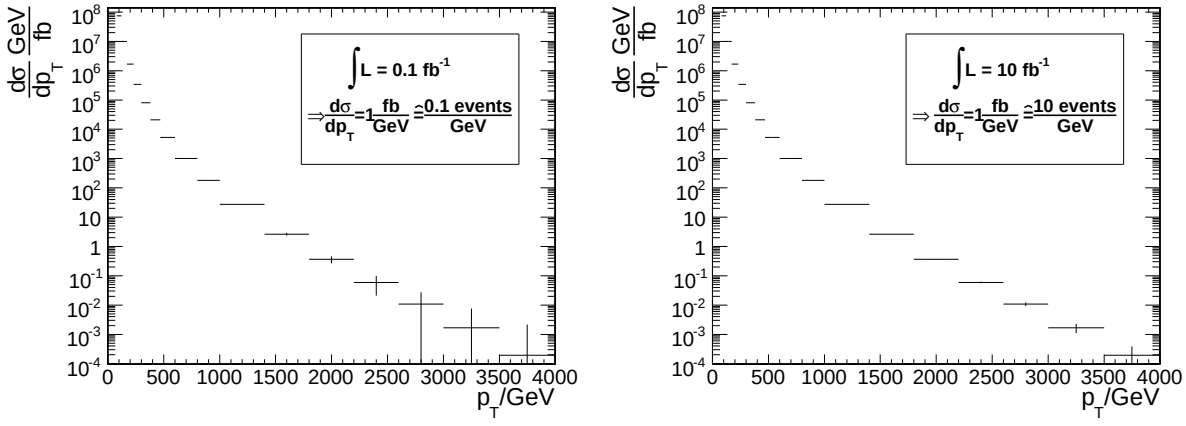

Figure 1: Expected statistical uncertainties on jet cross sections for a pilot run with $0.1\ \mathrm{fb}^{-1}$ (left) and for a first physics run with $10\ \mathrm{fb}^{-1}$. Note: The central cross section values are taken from a leading-order calculation and hence do not account for the statistical fluctuations present in the data.

In figure 2 a sketch of the proposed analysis is given. On the one hand side, the measured data have to be corrected for detector effects using fully simulated Monte-Carlo (MC) events. Subsequently, an energy calibration has to be performed on the reconstructed jets which ideally is extracted from data as well but can also be done employing Monte-Carlo methods. On the other hand, for the theory predictions, which are most precise with respect to the hard parton-parton scattering amplitudes, effects of soft physics modelled in the form of parton showers and hadronization models with subsequent decays have to be taken into account. Once this is done, parameters of our current theory can be cross-checked or improved in precison by comparing the measured hadronic final state with the corrected theoretical predictions.

2 Jet algorithms

In QCD, the confinement does not allow coloured objects like quarks or gluons to be separated from each other by distances larger than about one fermi. The energy invested in the colour field between these partons is used up to create quark anti-quark pairs from the vacuum until all these partons have been integrated into colourless hadrons. As a consequence, collimated streams of hadrons, which are customarily named jets, are observed in a detector while at the origin a small number of partons had been created in the hard collision. In order to reestablish the link between the observed particles and the hard process, algorithms are defined to group particles that are supposed to come from the same hard parton into jets. The required ingredients of such a jet algorithm are:

1. a distance measure to define the separation between objects
2. a procedure how to decide when objects are to be combined
3. a recombination scheme explaining how to combine objects

In addition, it has to be specified how the list of input objects has been determined.

Two principal types are in common use: Cone type algorithms [5] that traditionally have been employed in hadron-hadron collisions where objects are clustered together that are close in angle around a high-energetic seed, and

[1)] Trigger pre-scales have been taken into account.

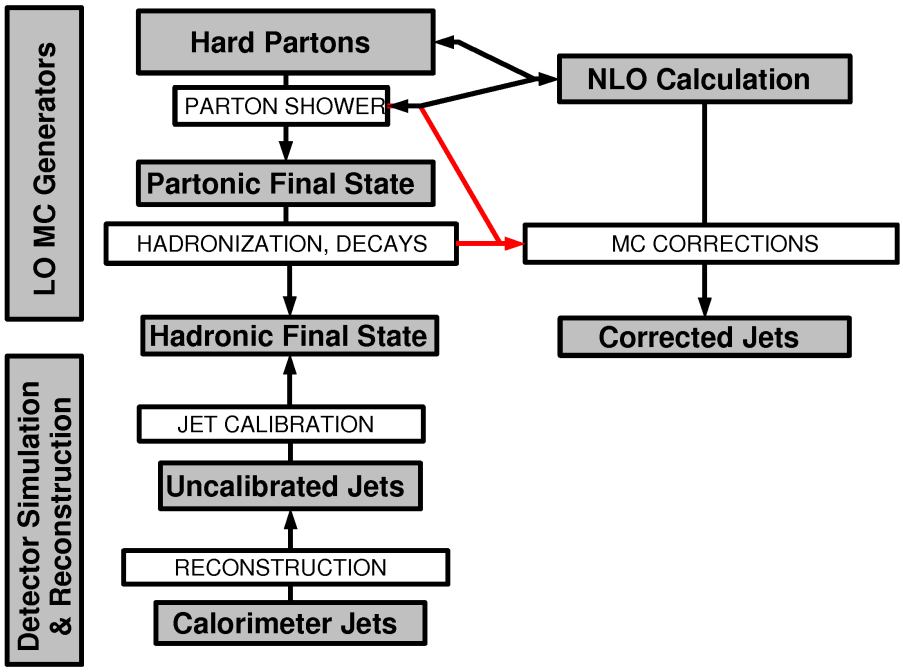

Figure 2: Analysis setup.

subsequent clustering algorithms where iteratively objects are combined that have the smallest distance of all pairwise combinations possible. The latter have predominantly been used in e^+e^- and $e^\pm p$ collisions, first in the form of the Jade algorithm [6, 7] and nowadays as k_T algorithm [8].

Before specifying the two versions applied in this study some commonalities are given. In both cases an angular distance measure will be used, the normally chosen angles are the azimuthal angle Φ and the pseudo-rapidity

$$\eta = -\ln\tan\frac{\Theta}{2}. \tag{1}$$

In recent publications [2, 9] though it has become an established standard to use the rapidity

$$y = \frac{1}{2}\ln\frac{E+p_z}{E-p_z} \tag{2}$$

instead of the pseudo-rapidity and this will also be followed here. The distance between two objects i and j hence reads

$$\Delta R_{ij} = \sqrt{(\Delta_{ij}\Phi)^2 + (\Delta_{ij}y)^2} \tag{3}$$

In addition, the most frequently used recombination scheme, the E scheme implying a simple four-vector addition, is employed in both cases.

The two types of jet algorithms finally used are:

1. Cone-type: Midpoint cone algorithm [10, 11] with:
   - Cone radius $R = 0.7$, all objects within a cone have to fulfill $R_{ic} \leq R$ with c labelling the four-vector of the current cone.
   - Overlap threshold $f_\mathrm{merge} = 0.50$, i.e. overlapping cone jets are merged when they share more than 50% of the energy in the less energetic cone
   - Search-cone radius fraction $f_\mathrm{search} = 0.5$, i.e. the first step to find the stable cones (before any splitting/merging is done) is performed with a smaller radius of $f_\mathrm{search} * R$
2. Iterative clustering-type: Inclusive k_T algorithm [12] with
   - Distances are evaluated according to the ΔR scheme, i.e. $d_{ij} = \min(p_{T,i}^2, p_{T,j}^2)\frac{\Delta R_{ij}^2}{D^2}$ with R_{ij} as in eq. 3

- Jet resolution parameter $D = 1.0$

Note, that primarily due to the limited choice of available jet energy calibrations the definitions above have been selected. In fact, cone type algorithms, although rather intuitively easy to understand, in general suffer from several short-comings. In addition to the problem of objects assigned to two cones (overlap) or none (dark jets) especially for comparisons to calculations in perturbative QCD they have to be infrared and collinear safe which was not the case for the Snowmass algorithm employed for analyzing jets in Run I at the Tevatron. To remedy this, the midpoint algorithm has been developed, for a complete discussion see reference [10]. As a modification of this algorithm, it was proposed in [11] to use smaller cone sizes in the phase where stable cones are searched for like defined above. But there have been indications that this again leads to an infrared sensitive behaviour [13] so it is recommended to use the original definition of the midpoint algorithm and not the one here.

Concerning the k_{T} algorithm a jet resolution parameter of $D = 1.0$ is, from a theoretical point of view, best comparable to a cone algorithm with $R = 0.7$. In order to reduce the sensitivity to the underlying event though it is advantageous to reduce the cone size R resp. the resolution parameter D which will be investigated in a future extension of this study.

3 Trigger scheme

The level one (L1) and the high level trigger (HLT) required for this analysis are the single jet triggers which are described in more detail in [1]. In the pilot phase with a luminosity $\mathcal{L}$ of $10^{32}\,\mathrm{cm}^{-2}\mathrm{s}^{-1}$ the relevant trigger paths lead to prescales of 2000 up to $60\ \mathrm{GeV}$ of offline corrected transverse jet energy (low path) and 40 up to $120\ \mathrm{GeV}$ (medium path). Above, no prescales are applied.

For first physics runs with a luminosity $\mathcal{L}$ of $10^{33}\,\mathrm{cm}^{-2}\mathrm{s}^{-1}$ the prescales are increased by a factor of ten, for jets of the high path this is valid up to transverse energies of $250\ \mathrm{GeV}$. In case of a doubled luminosity later on, this is reflected by the trigger settings by halving the corresponding rates up to the high trigger path.

The described settings have been chosen in order to ensure an efficiency of at least 95% at the HLT trigger thresholds. The expected statistical uncertainties on jet cross sections, where trigger pre-scales have been taken into account but not the trigger efficiencies, are presented in figure 1 for a pilot run with $0.1\ \mathrm{fb}^{-1}$ and for a first physics run with $10\ \mathrm{fb}^{-1}$. According to

$$\sigma = \frac{N_{\mathrm{jets}}}{\epsilon \int \mathcal{L}} \tag{4}$$

the statistics will be further reduced by factor of ϵ where ϵ is the efficiency of the corresponding single jet trigger at a given transverse jet energy E_{T} . For jets with an E_{T} larger than $350\ \mathrm{GeV}$ in the pilot run and resp. $500\ \mathrm{GeV}$ in a first physics run the efficiencies will practically be one. In the following all triggers are assumed to be fully efficient already at their respective thresholds, hence $\epsilon = 1$. In a later update, this has to be studied further.

4 Event selection and background

There is basically only one requirement in this study: All jets must have a transverse momentum larger than $50\ \mathrm{GeV}$. Since QCD jet production has by several orders of magnitude the largest cross section whatsoever detailed background studies are not necessary. In fact, to most analyses QCD jet events are the background.

Once, the real detector comes into play, the event selection process might become more involved in order to exclude effects due to misinterpretations of high energetic electrons or photons, incorrectly vertexed events, detector noise, accelerator losses or cosmic rays for example.

5 Phase space and binning

Starting with jets of a transverse momentum larger than $50\ \mathrm{GeV}$ the phase space is subdivided into five ranges in rapidity y, see table 1, and 34 ranges in transverse momentum p_{T}, see table 2. The binning in y is motivated by the structure of the CMS calorimeters. The bins in rapidity nos. 1 and 3 are fully contained in the barrel part resp. the endcaps of the CMS detector whereas bins no. 2 and 4 correspond to the transition regions. Finally, the last bin covers the kinematic range accessible by the forward detectors. In this study we concentrate mostly on the central region up to 2.5 in rapidity.

The binning in transverse momentum follows the one employed in the sets of simulated data that were investigated, see table 3 for details. For the purpose of the theory calculations of section 9 in each of these datasets the range in p_{T} was further subdivided into two intervals. Because of foreseen studies on trigger efficiencies, in two cases the subdivisions were set expressly at $60\ \mathrm{GeV}$ and $250\ \mathrm{GeV}$ reflecting the corresponding trigger thresholds.[2)] Later on it might be necessary, especially with respect to a proper treatment of bin-to-bin migrations and the jet energy resolution, to reevaluate this choice. The lowest range in p_{T} from 50 up to $80\ \mathrm{GeV}$ will not be taken into account for final results and is examined solely for the purpose of checking the behaviour at the edge of the phase space.

Table 1: Binning in rapidity y for high p_{T} jet cross sections. Within the scope of this note the analysis of the simulated data is restricted to the central bins up to a rapidity of 2.5.

Bin no.	Range in rapidity y
1	$0.00 \leq \lvert y \rvert < 0.75$
2	$0.75 \leq \lvert y \rvert < 1.50$
3	$1.50 \leq \lvert y \rvert < 2.50$
4	$2.50 \leq \lvert y \rvert < 3.00$
5	$3.00 \leq \lvert y \rvert < 5.00$

Table 2: Binning in transverse momentum p_{T} for the theory computation of the high p_{T} jet cross sections. In case of the simulated datasets every second bin of this table has to be merged with the previous one.

Bin no.	Range in p_{T}	Bin no.	Range in p_{T}	Bin no.	Range in p_{T}
1	$50. \leq p_{\mathrm{T}}/\ \mathrm{GeV} < 60.$	13	$380. \leq p_{\mathrm{T}}/\ \mathrm{GeV} < 425.$	24	$1600. \leq p_{\mathrm{T}}/\ \mathrm{GeV} < 1800.$
2	$60. \leq p_{\mathrm{T}}/\ \mathrm{GeV} < 80.$	14	$425. \leq p_{\mathrm{T}}/\ \mathrm{GeV} < 470.$	25	$1800. \leq p_{\mathrm{T}}/\ \mathrm{GeV} < 2000.$
3	$80. \leq p_{\mathrm{T}}/\ \mathrm{GeV} < 95.$	15	$470. \leq p_{\mathrm{T}}/\ \mathrm{GeV} < 520.$	26	$2000. \leq p_{\mathrm{T}}/\ \mathrm{GeV} < 2200.$
4	$95. \leq p_{\mathrm{T}}/\ \mathrm{GeV} < 120.$	16	$520. \leq p_{\mathrm{T}}/\ \mathrm{GeV} < 600.$	27	$2200. \leq p_{\mathrm{T}}/\ \mathrm{GeV} < 2400.$
5	$120. \leq p_{\mathrm{T}}/\ \mathrm{GeV} < 145.$	17	$600. \leq p_{\mathrm{T}}/\ \mathrm{GeV} < 700.$	28	$2400. \leq p_{\mathrm{T}}/\ \mathrm{GeV} < 2600.$
6	$145. \leq p_{\mathrm{T}}/\ \mathrm{GeV} < 170.$	18	$700. \leq p_{\mathrm{T}}/\ \mathrm{GeV} < 800.$	29	$2600. \leq p_{\mathrm{T}}/\ \mathrm{GeV} < 2800.$
7	$170. \leq p_{\mathrm{T}}/\ \mathrm{GeV} < 195.$	19	$800. \leq p_{\mathrm{T}}/\ \mathrm{GeV} < 900.$	30	$2800. \leq p_{\mathrm{T}}/\ \mathrm{GeV} < 3000.$
8	$195. \leq p_{\mathrm{T}}/\ \mathrm{GeV} < 230.$	20	$900. \leq p_{\mathrm{T}}/\ \mathrm{GeV} < 1000.$	31	$3000. \leq p_{\mathrm{T}}/\ \mathrm{GeV} < 3250.$
9	$230. \leq p_{\mathrm{T}}/\ \mathrm{GeV} < 250.$	21	$1000. \leq p_{\mathrm{T}}/\ \mathrm{GeV} < 1200.$	32	$3250. \leq p_{\mathrm{T}}/\ \mathrm{GeV} < 3500.$
10	$250. \leq p_{\mathrm{T}}/\ \mathrm{GeV} < 300.$	22	$1200. \leq p_{\mathrm{T}}/\ \mathrm{GeV} < 1400.$	33	$3500. \leq p_{\mathrm{T}}/\ \mathrm{GeV} < 3750.$
11	$300. \leq p_{\mathrm{T}}/\ \mathrm{GeV} < 335.$	23	$1400. \leq p_{\mathrm{T}}/\ \mathrm{GeV} < 1600.$	34	$3750. \leq p_{\mathrm{T}}/\ \mathrm{GeV} < 4000.$
12	$335. \leq p_{\mathrm{T}}/\ \mathrm{GeV} < 380.$				

6 Datasets and input selection

Two kinds of input have been examined, on the one hand datasets where the events were generated with PYTHIA and subsequently subjected to the full CMS detector simulation and reconstruction programs OSCAR and ORCA, see table 3 for details. On the other hand, datasets with only generated events by PYTHIA where the settings were chosen identical to the fully simulated ones. The latter was done in order to have efficient access to acceptable statistics for hadronization studies alone.

Corresponding to the analysis setup presented in figure 2, four classes of input objects to the jet algorithms have been considered: The initial partons of the hard interaction, partons after parton shower (partonic final state, PFS) all stable particles of the hadronic final state (HFS) other than muons or neutrinos and calorimeter towers. The classes of MC objects were also analyzed in dedicated generator studies with sets of about 100000 events for each range in p_{T} as given by the simulated datasets (in total $1.7M$ events). With the fully simulated events one is able to examine in detail how energy deposits measured in the calorimeter towers of the electromagnetic and hadronic calorimeters can be related to the generator event. For this purpose, calorimeter towers fulfilling the requirements

1. $E > 0.8\ \mathrm{GeV}$
2. $E_{\mathrm{T}} > 0.5\ \mathrm{GeV}$

[2)] At the trigger threshold of $120\ \mathrm{GeV}$ there was a division already anyway.

were subjected to the same jet algorithms as the generator particles. Subsequently they were matched by looking for the pairs of generator and calorimeter jets closest to each other in distance $d = \sqrt{(\Delta\Phi)^2 + (\Delta\eta)^2}$. For this study, 20000 events of each dataset were used.

Table 3: Datasets used. The numbers in the dataset names correspond to the range of allowed values for $\hat{p}_T$ of the hard interaction (`CKIN 3, CKIN 4`).

Datasets	No. of generated events	No. of evaluated events	PYTHIA LO cross section/mb
jm03b_qcd_50_80	200k	20k	2.094E-2
jm03b_qcd_80_120	300k	20k	2.950E-3
jm03b_qcd_120_170	300k	20k	4.997E-4
jm03b_qcd_170_230	400k	20k	1.010E-4
jm03b_qcd_230_300	300k	20k	2.386E-5
jm03b_qcd_300_380	200k	20k	6.391E-6
jm03b_qcd_380_470	200k	20k	1.890E-6
jm03b_qcd_470_600	200k	20k	6.902E-7
jm03b_qcd_600_800	100k	20k	2.025E-7
jm03b_qcd_800_1000	100k	20k	3.574E-8
jm03b_qcd_1000_1400	100k	20k	1.085E-8
jm03b_qcd_1400_1800	50k	20k	1.056E-9
jm03b_qcd_1800_2200	50k	20k	1.448E-10
jm03b_qcd_2200_2600	50k	20k	2.382E-11
jm03b_qcd_2600_3000	50k	20k	4.285E-12
jm03b_qcd_3000_3500	40k	20k	8.440E-13
jm03b_qcd_3500_4000	40k	20k	9.654E-14

7 Jet energy calibration

Two techniques for the jet energy calibration have been proposed, a MC calibration based on the comparison of matched calorimeter and generator jets derived from the hadronic final state, and a gamma-jet calibration where jet transverse energies are measured against recoiling high energetic photons. Within the version of the detector reconstruction employed in this study[3)] the gamma-jet calibration method exhibited a strange behaviour and was henceforth discarded.

The MC calibration method implies calibration factors, applied on a jet by jet basis to the calorimeter jets, depending on pseudo-rapidity η and transverse momentum p_{T}.

8 Experimental uncertainties

From the experience at the Tevatron, see for example the latest CDF and D0 publications [2, 3, 14], it is known that the relevant sources for the experimental uncertainty of high p_{T} jet cross section measurements are, in order of importance:

1. the jet energy scale
2. the jet energy resolution
3. the unfolding of the measured cross section to the hadronic final state
4. the luminosity

By far dominant is the jet energy scale where an uncertainty of 3% results in uncertainties on the jet cross sections of about 10% at low p_{T} up to 60% at high p_{T}. Each other contribution remains below 10% in the whole range of accessible p_{T}. Due to tight infrastructural (data access, grid performance and reliability) as well as timing limitations (readiness of indispensable tools) we restrict ourselves to only the most important point. A more complete uncertainty study has to follow later on.

[3)] ORCA release 8.7.4

According to CMS recommendations the jet energy scale in this analysis has been varied by $\pm 3\%$ in order to estimate the impact on the cross section determination. Figure 3 shows the average relative differences in jet energy between MC calibrated and HFS jets derived with the k_{T} algorithm. Apart from the borders of the phase space with very low statistics at very high p_{T} or at the border where jets with a transverse momentum smaller than $50\ \mathrm{GeV}$ are cut out it can be seen that on average the discrepancies are well below 3%. Since a MC calibration technique was employed, in fact, one would not expect anything else. Due to details of this procedure probably some features remain to be seen especially at the edges of the calorimeters like the undercalibrated bands at rapidities of about 1.3 and 3.0. Also, in the range between 2.0 and 2.8 a slight overcalibration is exhibited. Figure 5 finally presents on the left hand side the relative experimental uncertainty on the jet cross section due to a variation in jet energy scale of $\pm 3\%$ for three regions in rapidity. Starting at about 15% at low p_{T} it rises up to about 50% at high p_{T} for central rapidity. In the two non-central rapidiy regions the uncertainties are of an equal size below about $1\ \mathrm{TeV}$ of transverse momentum, but get considerably larger for higher p_{T}. In general, a similar behaviour is observed as can be expected from Tevatron results.

Another source of uncertainty considered is a systematic shift in the reconstructed polar angle (or pseudo-rapidity)[4] of the jets compared to their original direction. In case of a simple displacement of the average z vertex position with respect to the detector no large impact is expected due to cancelling effects between the jet p_{T} measurements in the forward and backward directions. On the contrary, the granular structure of the calorimeter and the material before it may lead, depending on the polar angle, to reconstructed jet transverse momenta which are too small (or too large) on both sides of the detector. Three scenarios labelled $(-,+)$, $(+,+)$ and $(+,-)$ have been considered where the labels indicate whether the quantity $\Delta\eta > 0$ is added or subtracted $(\pm,.)$ with respect to jets in the backward direction $(\eta < 0)$ resp. forward direction $(\eta > 0)$: $(.,\pm)$. The $(-,+)$ scenario therefore corresponds to a systematic underestimation of jet transverse momenta, the $(+,-)$ scenario to a systematic overestimation and the $(+,+)$ scenario to a mixed case like with a shifted z vertex.

In figure 4 the average differences in pseudo-rapidity between MC calibrated and HFS jets are shown where on the right hand side the shown range in $\Delta\eta$ is reduced to ± 0.01 with respect to ± 0.04 on the left hand side. No large systematic effect is observed. Nevertheless the impact on the jet cross sections was studied by assuming systematic shifts in pseudo-rapidity of 0.01 for $(0.0 \leq |\eta| < 2.0)$ and 0.05 for $(2.0 \leq |\eta|)$. The result is presented in figure 5 on the right hand side and reveals an impact of maximally 12% at low p_{T} for jets of all rapidities.

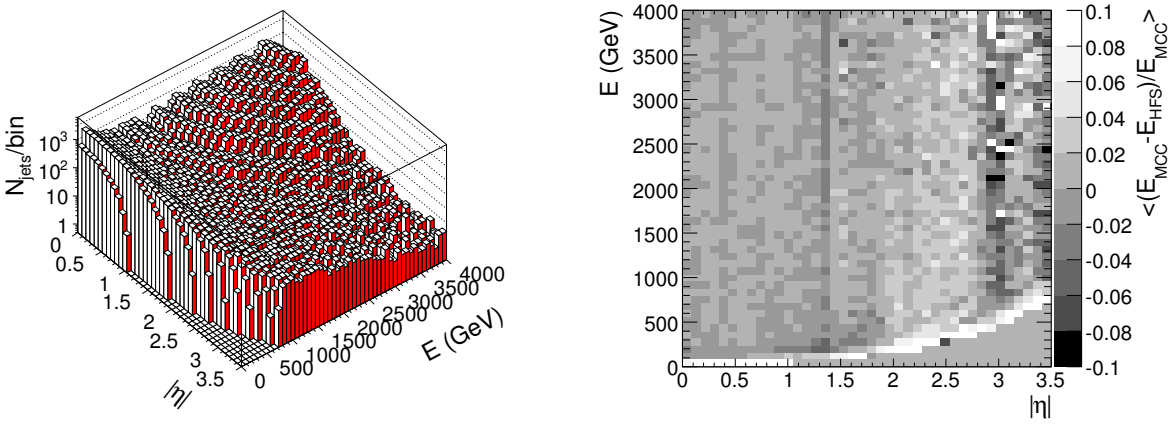

Figure 3: On the left hand side the available statistics for the comparison on the right and for figure 4 is shown. On the right hand side, average relative differences in jet energy between MC calibrated and HFS jets derived with the k_{T} algorithm are presented. Only the two matched jets with highest p_{T} are compared.

In the low transverse momentum region the influence of the underlying event and multiple interactions constitute another source of uncertainty. In the latest CDF publication [2] it was estimated to decrease the cross section by 22% at low p_{T} but only 4% at high transverse momentum. In addition, this effect was observed to be partially cancelled by hadronization corrections that increase the cross section again by 13% resp. 3.5%. Larger effects up to even higher transverse momenta can be expected within the dense environment of LHC collisions. This has not been studied yet and will be one of the major concerns in the next future.

[4] Note that the jet algorithms are still applied using the rapidity y!

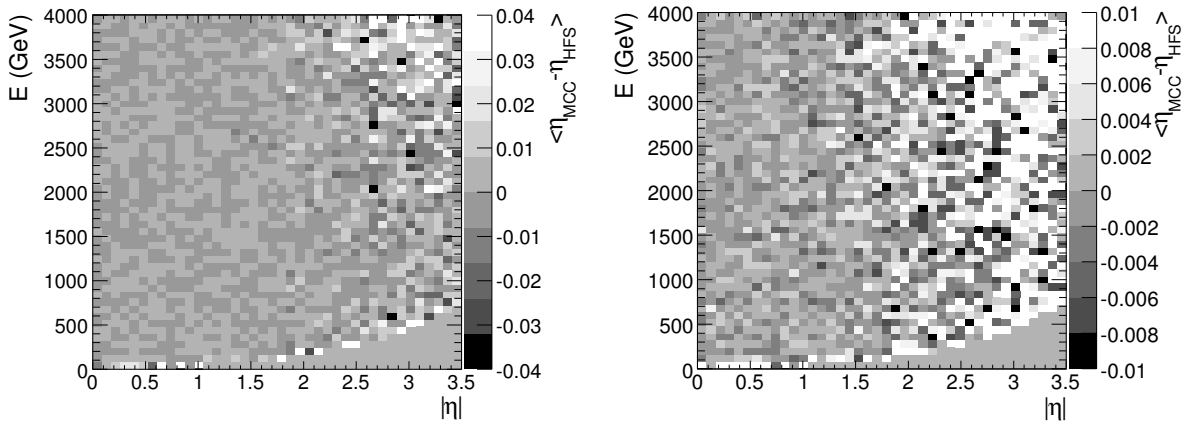

Figure 4: Average differences in pseudo-rapidity between MC calibrated and HFS jets derived with the k_{T} algorithm. Only the two matched jets with highest p_{T} are compared. On the right hand side the shown range in $\Delta\eta$ is reduced to ± 0.01 with respect to ± 0.04 on the left hand side leading to white squares representing also under- and overflows.

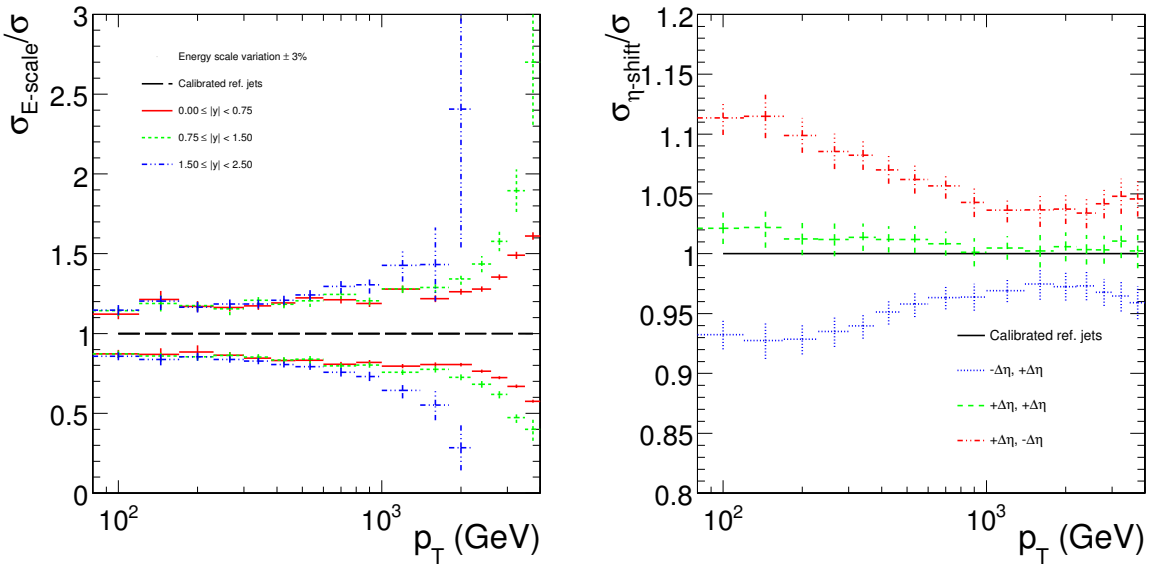

Figure 5: Relative systematic uncertainties of the jet cross sections for the k_{T} algorithm versus p_{T} due to a change in energy scale of $\pm 3\%$ for three bins in rapidity (left) and due to shifts in pseudo-rapidity of 0.01 $(0.0 \leq |\eta| < 2.0)$ resp. 0.05 $(2.0 \leq |\eta|)$. The labels $(-,+)$, $(+,+)$, $(+,-)$ indicate whether the quantity $\Delta\eta > 0$ is added or subtracted $(\pm,.)$ with respect to jets in the backward direction $(\eta < 0)$ resp. forward direction $(\eta > 0)$: $(.,\pm)$. Jets of all rapitidies were considered for the plot on the right hand side. The error bars represent the statistical uncertainty. Similar results have been observed for the midpoint cone algorithm.

Finally, the luminosity measurement leads to an uncertainty in the total normalization of the jet cross sections, which amounts for example in [2] to 6%, and leads to a systematic shift to the left or right of the whole differential cross section. Deviations of the the high p_{T} cross section from theoretical calculations could be established nevertheless by normalizing to the region of low transverse momenta.

9 NLO calculation

In order to compare to theoretical predictions of perturbative QCD calculations of at least next-to-leading order (NLO) precision are required. As input the parton density functions (PDFs) of the proton and a value for the coupling of the strong interaction α_S are needed. This leads to three sources of theoretical uncertainty where the impact of the parton density functions is expected to be the by far largest contribution in case of high p_{T} jet cross sections:

1. Uncertainty of the measured input parton density functions
2. Uncertainty of the strong coupling α_S
3. Uncertainty of the fixed order calculations, conventionally estimated by varying the (unphysical) renormalization and factorization scales

For the NLO calculation the program NLOJET++ [15] is employed. However, since precise computations in NLO are very time consuming, a more efficient set-up in the form of the fastNLO project [16] is used which allows the fast rederivation of the considered cross section for arbitrary input PDFs and α_S values. This is done by separating the PDF dependency from the hard matrix element calculation by interpolating the PDFs between fixed support points in fractional proton momentum x so that the PDF dependency can be evaluated a posteriori from one complete calculation.

Note that neither PYTHIA nor NLOJET++ contain electroweak corrections which may change high p_{T} cross sections from 1 TeV onwards up to 30% [17]. Insofar this study is consistent but before comparing to real data this has to be taken into account.

To illustrate the influence of the PDFs, figure 6 shows the decomposition of the total jet cross section into the seven possible partonic subprocesses for $p\bar{p}$ collisions at the Tevatron on the left hand side and for pp collisions at the LHC on the right hand side at central rapidities. The fractional contributions are drawn versus the scaling variable $x_T = 2p_{\mathrm{T}}/\sqrt{s}$. As expected large percentages from gluon induced processes can be seen in the low p_{T} region. The higher the transverse momentum the more $q\bar{q}$ in case of the Tevatron and qq partonic reactions in case of the LHC dominate. One has to keep in mind though that due to sum rules the PDFs are coupled and cannot be considered separately.

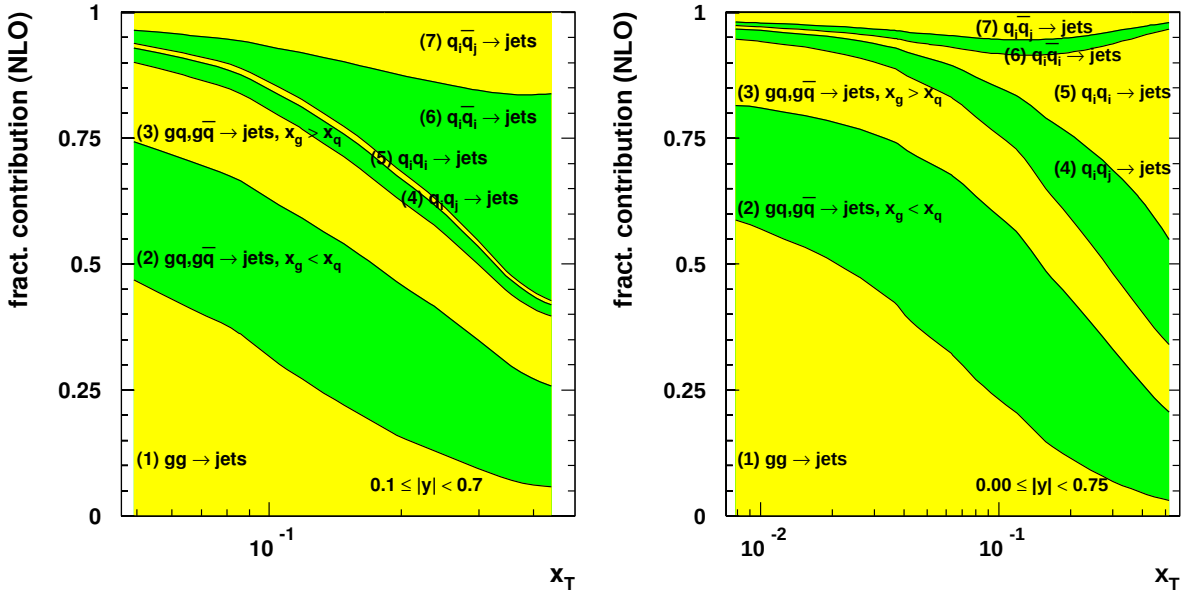

Figure 6: Decomposition of the total jet cross section into the partonic processes for $p\bar{p}$ collisions at the Tevatron (left) resp. pp collisions at the LHC (right). The fractional contributions are shown versus the scaling variable $x_T = 2p_{\mathrm{T}}/\sqrt{s}$.

In figure 7 on the left hand side the double-differential high p_{T} jet cross section at NLO for the five rapidity ranges of table 1 is presented. The thickness of the coloured bands correspond to the total uncertainty due to an evaluation of the 40 error sets of the CTEQ6M [4] PDFs in comparison to the central one. On the right hand side, the relative uncertainties for the three innermost rapidities are shown. The total uncertainty ranges from a minimum of about 5% at medium transverse momenta up to 65% at highest p_{T} in case of the central rapity region. For larger rapidities up to $|y| = 2.50$ it becomes even more than twice as large.

In order to have a closer look onto the origin of the PDF uncertainty the decomposition relative to the total cross section into the four components $gg \to$ jets, $gq, g\bar{q} \to$ jets $(x_g < x_q)$, $gq, g\bar{q} \to$ jets $(x_g > x_q)$ and the maximum of any $qq, q\bar{q} \to$ jets subprocess is displayed in figure 8 for two different rapidity regions.[5)] As expected

the dominant contribution comes from gluon induced processes but not necessarily from $gg \to \text{jets}$ alone. At sufficiently high p_{T} the subprocesses $gq, g\bar{q} \to \text{jets}$ become even the larger ones owing to their large contribution to the total cross section, see figure 6. In addition, it can be concluded that the gluon induced uncertainties of the jet cross section increase with rising rapidity.

Uncertainties due to the strong coupling and scale variations have been observed to be small compared to the PDF uncertainty.

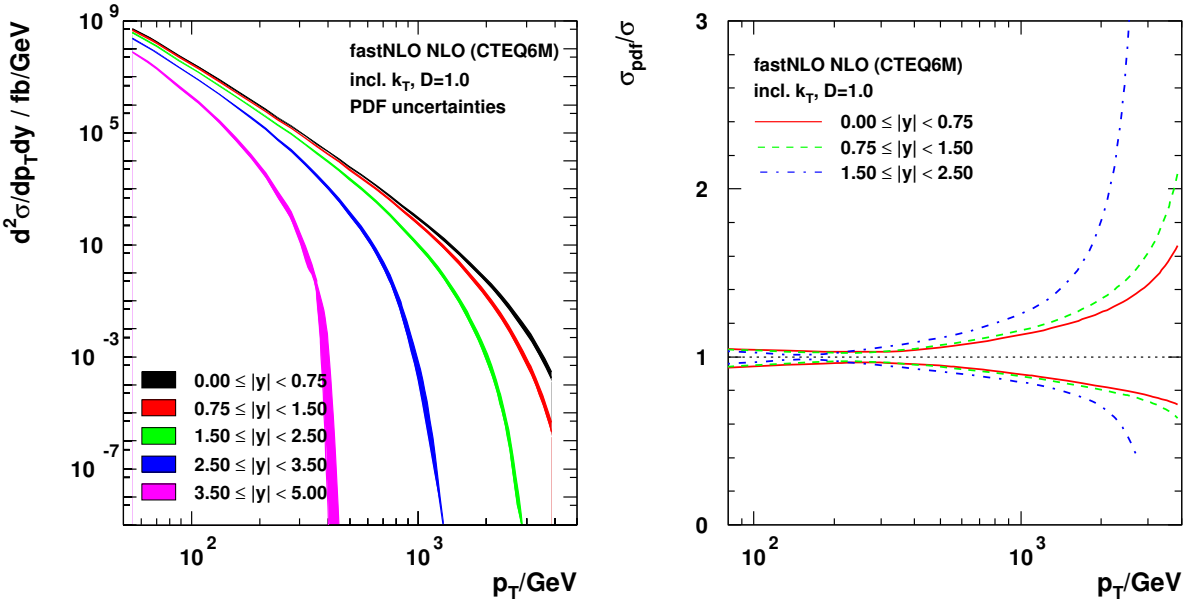

Figure 7: Double-differential high p_{T} jet cross section at NLO for the five rapidity ranges of table 1. The thickness of the coloured bands correspond to the total uncertainty due to an evaluation of the error sets of the CTEQ6M [4] PDFs. On the right hand side, the relative uncertainties for the three innermost rapidities are shown.

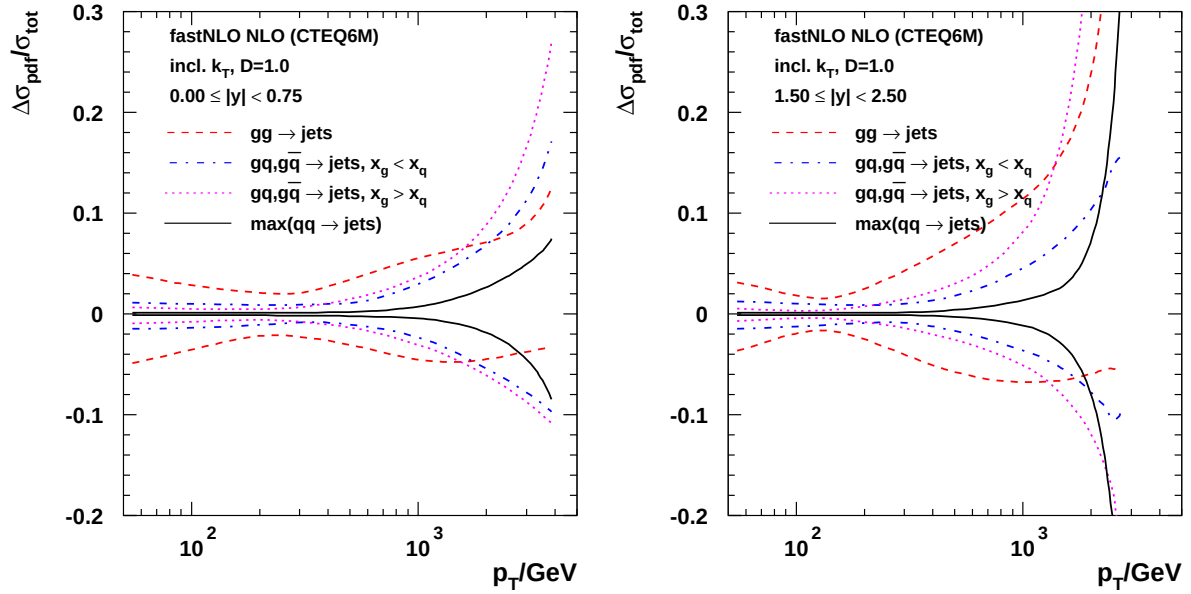

Figure 8: Decomposition of the PDF uncertainty relative to the total cross section into the four components $gg \to \text{jets}$, $gq, g\bar{q} \to \text{jets}$ $(x_g < x_q)$, $gq, g\bar{q} \to \text{jets}$ $(x_g > x_q)$ and the maximum of any $qq, q\bar{q} \to \text{jets}$ subprocess. On the left hand side this is shown for rapidities of $0.00 \leq |y| < 0.75$ and on the right hand side for $1.50 \leq |y| < 2.50$.

[5] Note that due to correlations between the PDFs the uncertainties of the different subprocesses can not simply be added to give the total uncertainties of figure 7.

10 Hadronization corrections

As a last point it has to be remembered that NLO calculations can not be compared directly to calibrated calorimeter jets that have been corrected for detector effects. In addition, the influence of the parton shower, hadronization and decays has to be estimated and correction factors have to be applied to the NLO result. As can be seen from figure 2 this can unfortunately not yet been done in a completely consistent manner since the MC generation programs, PYTHIA as well as HERWIG, do only allow for LO matrix elements to be coupled to parton showers and the subsequent hadronization. Keeping this in mind, the following procedure was followed in order to estimate this correction.

In order to check the transition from after parton showering (partonic final state, PFS) to the hadronic final state, which is comparable to calibrated detector jets, within the MC information all partonic like objects (gluons, quarks, anti-quarks, diquarks) that enter into the string fragmentation phase are used as input to the jet algorithms as well. With this tool in hand we can now check the ratio of the inclusive jet cross sections for the hadronic and the partonic final state. The result is shown in figure 9 where correction factors of the order of 1% are observed. In order to be less model dependent this exercise should be repeated using e.g. the HERWIG MC program employing the cluster instead of string fragmentation model for hadronization. This has not yet been done.

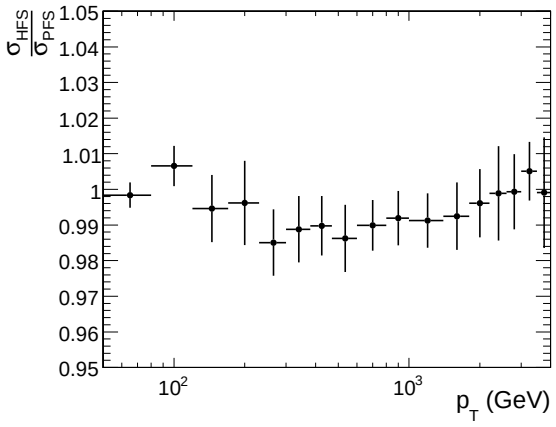

Figure 9: Hadronization corrections to the high p_{T} jet cross sections have been derived with PYTHIA. They are observed to be of the order of 1%.

11 Conclusions

The dominant experimental and theoretical uncertainties on the differential inclusive cross sections of jets with high transverse momentum ranging from $80\ \mathrm{GeV}$ up to $4000\ \mathrm{GeV}$ have been investigated. A variation of $\pm 3\%$ in the jet energy scale of the CMS calorimeters results in an uncertainty of the derived jet cross sections of 15% at low transverse momenta increasing up to about 50% at the highest p_{T}. The theoretical uncertainty due to the parton density functions of the proton has been found to be of the same order of magnitude and rises from about 5% for low transverse momenta with a minimum of 3% at $\approx 200\ \mathrm{GeV}$ up to $+65\%$ and -30% at the highest transverse momenta. Most results have been shown for the k_{T} jet algorithm. The basic conclusions are equally valid for the midpoint cone algorithm where similar results were obtained.

A couple of sources of experimental uncertainty, each at the below 10% level, especially the jet energy resolution, the unfolding of bin-to-bin migrations, corrections due to the underlying event and multiple interactions, trigger efficiencies and the luminosity normalisation have been neglected and will be the subject of further studies. On the theory side, corrections when going from the QCD calculation in fixed order to the hadronic final state still have to be taken into account. Ideally, this would be done using NLO calculations that allow to attach parton showers so that only hadronization corrections have to be derived from LO MC programs like PYTHIA or HERWIG. In addition, electroweak corrections have to be included before comparing to real data.

Once the study of the remaining uncertainties has been finished, it will be possible to run simultaneous fits of α_S and the parton density functions, especially the gluon density at high x, to the data. Depending on the exact performance of the detector and the precision of the jet energy scale the impact of the LHC jet data might be limited. This can be improved upon by extending the range in rapidity from just the central one, looking at other jet related quantities e.g. jet rates, or by including other processes into the fit procedure like W/Z production as luminosity measure or Drell-Yan reactions to fix the low x gluon density.

References

[1] **CMS** Collaboration, D. Acosta et al., eds., "CMS Physics Technical Design Report", volume II. CERN, Geneva, Switzerland, 2006, to be published.

[2] **CDF Run II** Collaboration, A. Abulencia et al., "Measurement of the inclusive jet cross section in p anti-p interactions at s**(1/2) = 1.96-TeV using a cone-based jet algorithm," arXiv:hep-ex/0512020.

[3] **D0** Collaboration, V. M. Abazov et al., "The inclusive jet cross-section in p anti-p collisions at s**(1/2) = 1.8-TeV using the k(T) algorithm," *Phys. Lett.* **B525** (2002) 211–218, arXiv:hep-ex/0109041.

[4] J. Pumplin et al., "New generation of parton distributions with uncertainties from global QCD analysis," *JHEP* **07** (2002) 012, arXiv:hep-ph/0201195.

[5] G. Sterman and S. Weinberg, "JETS FROM QUANTUM CHROMODYNAMICS," *Phys. Rev. Lett.* **39** (1977) 1436.

[6] **JADE** Collaboration, W. Bartel et al., "EXPERIMENTAL STUDIES ON MULTI - JET PRODUCTION IN e+ e- ANNIHILATION AT PETRA ENERGIES," *Z. Phys.* **C33** (1986) 23.

[7] **JADE** Collaboration, S. Bethke et al., "EXPERIMENTAL INVESTIGATION OF THE ENERGY DEPENDENCE OF THE STRONG COUPLING STRENGTH," *Phys. Lett.* **B213** (1988) 235.

[8] S. Catani, Y. L. Dokshitzer, M. Olsson, G. Turnock, and B. R. Webber, "New clustering algorithm for multi - jet cross-sections in e+ e- annihilation," *Phys. Lett.* **B269** (1991) 432–438.

[9] **D0** Collaboration, R. Strohmer, "Inclusive jet cross-sections and dijet azimuthal decorrelations with D0," *PoS* **HEP2005** (2006) 051, arXiv:hep-ex/0601016.

[10] U. Baur, R. K. Ellis, and D. Zeppenfeld, eds., "QCD and Weak Boson Physics in Run II". FERMILAB, Batavia, IL, USA, 2000. Prepared for Physics at Run II: QCD and Weak Boson Physics Workshop: Final General Meeting, Batavia, Illinois, 4-6 Nov 1999.

[11] S. D. Ellis, J. Huston, and M. Tonnesmann, "On building better cone jet algorithms," *eConf* **C010630** (2001) P513, arXiv:hep-ph/0111434.

[12] J. M. Butterworth, J. P. Couchman, B. E. Cox, and B. M. Waugh, "KtJet: A C++ implementation of the K(T) clustering algorithm," *Comput. Phys. Commun.* **153** (2003) 85–96, arXiv:hep-ph/0210022.

[13] M. Wobisch, "private Communication.".

[14] **D0** Collaboration, B. Abbott et al., "High-p(T) jets in anti-p p collisions at s**(1/2) = 630-GeV and 1800-GeV," *Phys. Rev.* **D64** (2001) 032003, arXiv:hep-ex/0012046.

[15] Z. Nagy, "Three-jet cross sections in hadron hadron collisions at next-to-leading order," *Phys. Rev. Lett.* **88** (2002) 122003, arXiv:hep-ph/0110315.

[16] T. Kluge, K. Rabbertz, and M. Wobisch, "fastNLO - fast pQCD calculations for hadron-induced processes." http://hepforge.cedar.ac.uk/fastnlo. to be published.

[17] S. Moretti, M. R. Nolten, and D. A. Ross, "Weak corrections and high E(T) jets at Tevatron," arXiv:hep-ph/0503152.